THE JOURNAL OF BIOLOGICAL CHEMISTRY VOL. 281, NO. 49, pp. 37930–37941, December 8, 2006
Printed in the U.S.A.

Structural Snapshots of *Escherichia coli* Histidinol Phosphate Phosphatase along the Reaction Pathway*

Received for publication, May 22, 2006, and in revised form, August 8, 2006 Published, JBC Papers in Press, September 11, 2006, DOI 10.1074/jbc.M604916200

Erumbi S. Rangarajan[‡], Ariane Proteau[‡], John Wagner[§], Ming-Ni Hung[§], Allan Matte[§¶1], and Miroslaw Cygler[‡§2]

From the [‡]Department of Biochemistry, McGill University, Montréal, Québec H3G 1Y6, Canada, the [§]Biotechnology Research Institute, National Research Council of Canada, Montréal, Québec H4P 2R2, Canada, and the [¶]Department of Immunology and Microbiology, McGill University, Montréal, Québec H3A 2B4, Canada

HisB from *Escherichia coli* is a bifunctional enzyme catalyzing the sixth and eighth steps of L-histidine biosynthesis. The N-terminal domain (HisB-N) possesses histidinol phosphate phosphatase activity, and its crystal structure shows a single domain with fold similarity to the haloacid dehalogenase (HAD) enzyme family. HisB-N forms dimers in the crystal and in solution. The structure shows the presence of a structural Zn^{2+} ion stabilizing the conformation of an extended loop. Two metal binding sites were also identified in the active site. Their presence was further confirmed by isothermal titration calorimetry. HisB-N is active in the presence of Mg^{2+}, Mn^{2+}, Co^{2+}, or Zn^{2+}, but Ca^{2+} has an inhibitory effect. We have determined structures of several intermediate states corresponding to snapshots along the reaction pathway, including that of the phosphoaspartate intermediate. A catalytic mechanism, different from that described for other HAD enzymes, is proposed requiring the presence of the second metal ion not found in the active sites of previously characterized HAD enzymes, to complete the second half-reaction. The proposed mechanism is reminiscent of two-Mg^{2+} ion catalysis utilized by DNA and RNA polymerases and many nucleases. The structure also provides an explanation for the inhibitory effect of Ca^{2+}.

The histidine biosynthetic pathway serves as a model system for better understanding of the fundamental metabolic, physiological, and genetic processes in bacteria (1). This pathway is identical in both *Escherichia coli* and *Salmonella typhimurium* and has been thoroughly characterized (1, 2). The sixth and eighth steps of histidine biosynthesis are catalyzed by imidazole glycerol phosphate dehydratase (IGPD,[3] EC 4.2.1.19) and histidinol phosphate phosphatase (HPase, EC.3.1.3.15) respectively (1) (Scheme 1). In protobacteria, including *E. coli* and *S. typhimurium*, the IGPD and HPase activities are encoded by a single gene (3–5), whereas in archaea, eukarya, and most bacteria they are encoded by two separate genes (3). The bifunctional HisB enzyme has been proposed to be the result of a fusion of two independent cistrons that occurred recently in evolution (3).

Biochemical and genetic studies of the HisB enzyme together suggest that both of its enzymatic activities are independent of one another and reside in separate domains (6–8). The HPase activity is found within the N-terminal domain (residues 1–167, HisB-N), whereas the C-terminal domain (residues 168–356) exhibits the IGPD activity. The phosphatase activity requires the presence of metal ions such as Mg^{2+}, Mn^{2+}, Co^{2+}, or Zn^{2+} but is inhibited by calcium (9). Based on the presence of four invariant aspartic acid residues, HisB has been classified as a member of the haloacid dehalogenase-like hydrolase (HAD) family within the "DDDD" superfamily of aspartyl-phosphate utilizing phosphohydrolases/phosphotransferases (10, 11). The phosphoryl transfer catalyzed by phosphotransferases and phosphatases from the HAD family occurs via a phosphoaspartate intermediate and involves one metal ion (12). In the first half-reaction the catalytic aspartate (first in the conserved **D***X***D***X*(T/V) motif I) aided by the metal ion attacks the phosphorus leading to cleavage of the substrate phosphoester bond, formation of a phosphoaspartate intermediate, and the release of product. The second aspartate plays the role of general acid to protonate the leaving group (13). A conserved Ser/Thr present in motif II is involved in binding the phosphoryl group. The consensus sequence (G/S)**D***XX*(N/T)**D** comprises motif III in which the first aspartate is involved in metal coordination while the second aspartate in involved in orienting a lysine residue that in turn interacts with the phosphoryl group. In the second half-reaction, a water molecule activated by a general base (second aspartate of motif I) attacks the phosphoaspartate intermediate regenerating the active site aspartate and releasing inorganic phosphate. The other members of the DDDD superfamily

* This work was supported by the Canadian Institutes of Health Research Grant 200103GSP-90094-GMX-CFAA-19924 (to M. C.). Financial support for beamline X8C of the National Synchrotron Light Source comes principally from the Office of Biological and Environmental Research and of Basic Energy Sciences of the U.S. Dept. of Energy, and the National Center for Research Resources of the National Institutes of Health. The costs of publication of this article were defrayed in part by the payment of page charges. This article must therefore be hereby marked "*advertisement*" in accordance with 18 U.S.C. Section 1734 solely to indicate this fact.

The atomic coordinates and structure factors (codes 2FPR, 2FPS, 2FPU, 2FPW, and 2FPX) have been deposited in the Protein Data Bank, Research Collaboratory for Structural Bioinformatics, Rutgers University, New Brunswick, NJ (http://www.rcsb.org/).

[1] To whom correspondence may be addressed: Biotechnology Research Institute, 6100 Royalmount Ave., Montreal, Quebec H4P 2R2, Canada. Tel.: 514-496-2557; Fax: 514-496-5143; E-mail: allan.matte@nrc-cnrc.gc.ca.

[2] To whom correspondence may be addressed: Biotechnology Research Institute, 6100 Royalmount Ave., Montreal, Quebec H4P 2R2, Canada. Tel.: 514-496-6321; Fax: 514-496-5143; E-mail: mirek.cygler@nrc-cnrc.gc.ca.

[3] The abbreviations used are: IGPD, imidazole glycerol phosphate dehydratase; HPase, histidinol phosphate phosphatase; HisB-N, N-terminal domain of a bifunctional enzyme catalyzing the sixth and eighth steps of L-histidine biosynthesis; HAD, haloacid dehalogenase; ESI-MS, electrospray ionization-mass spectrometry; Bis-Tris, 2-[bis(2-hydroxyethyl)-amino]-2-(hydroxymethyl)propane-1,3-diol; ITC, isothermal titration calorimetry; AphA, acid phosphatase.

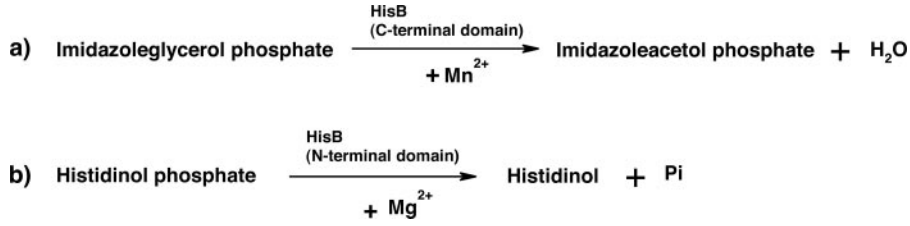

SCHEME 1. **General reaction catalyzed by the C-terminal IGPD domain of HisB (*a*) and the N-terminal HPase domain (*b*).**

include nonspecific phosphatases, phosphoglycolate phosphatases, phosphoserine phosphatases, and trehalose-6-phosphatases (3). Several enzymes belonging to the HAD family have been structurally and enzymatically characterized, including phosphoserine phosphatase from *Methanococcus jannaschii* (14), class B acid phosphatase from *E. coli* (15), human mitochondrial deoxyribonucleotidase (16), β-phosphoglucomutase from *Lactococcus lactis* (17, 18), and DNA 3′-phosphatase from *Saccharomyces cerevisiae* (19).

Interestingly, some bacteria utilize an unrelated enzyme to catalyze the same histidinol phosphate phosphatase reaction. Unlike *E. coli* HisB, this enzyme is monofunctional and belongs to the polymerase and histidinol phosphatase superfamily characterized by the presence of four conserved motifs, each containing a histidine residue (20). Members of the polymerase and histidinol phosphatase superfamily (*e.g.* HisB from *Thermus thermophilus* HB8 (21)) are structurally unrelated to the HAD family enzymes and employ a different catalytic mechanism.

The enzymes involved in the histidine biosynthesis pathway have recently been the subjects of intense structural investigation with crystal structures of all the *E. coli* enzymes (or their close orthologs) having been determined, with the exception of HPase (HisB-N). Here we report the crystal structures of *E. coli* HisB-N and several enzyme-ligand complexes. Based on these structures and the accompanying biochemical data we propose a novel mechanism for the dephosphorylation of histidinol phosphate mediated by two Mg^{2+} ions. This proposed mechanism is distinct from that previously reported for other HAD family enzymes, where only one Mg^{2+} ion is required for catalysis. We also show that in the presence of Ca^{2+} the reaction is arrested following the formation of the phosphoaspartate intermediate.

MATERIALS AND METHODS

Cloning, Mutagenesis, and Purification—The N-terminal domain of HisB (residues 3–166, gi: 12516203) from *E. coli* O157:H7 (22) was cloned into a modified pET15b vector (EMD Biosciences, San Diego, CA), yielding a fusion protein with an N-terminal extension $MGSS(H)_6GS$- and expressed in *E. coli* BL21(DE3). Site-directed mutagenesis of HisB-N ($Asp^{12} \rightarrow$ Ala, $Asp^{12} \rightarrow$ Ser, $Glu^{18} \rightarrow$ Ala, and $Glu^{18} \rightarrow$ Ser) was performed using the QuikChange™ kit (Stratagene, La Jolla, CA). Mutants were verified by DNA sequence analysis and ESI-MS of purified mutant proteins.

A 1-liter culture was grown in LB medium containing 100 μg ml^{-1} ampicillin for 2 h at room temperature, protein expression was induced with 100 μM isopropyl 1-thio-β-D-galactopyranoside, and the culture was incubated for an additional 6 h. Cell pellets were resuspended in 40 ml of lysis buffer (50 mM Tris-HCl (pH 7.5), 10 mM imidazole, 400 mM NaCl, 5% (v/v) glycerol, 10 mM β-mercaptoethanol, Complete™ protease inhibitor mixture (Roche Diagnostics, Laval, Canada) and 1% (v/v) Triton X-100) and sonicated on ice for a total of 2 min with cycles of 15 s on and 15 s off. The lysate was centrifuged at 100,000 × *g* for 40 min at 4 °C, and the supernatant was incubated with DEAE-Sepharose (Amersham Biosciences) pre-equilibrated with the lysis buffer. The flow-through was loaded on a 1-ml nickel-nitrilotriacetic acid column (Qiagen, Valencia, CA), washed with buffer (50 mM Tris-HCl (pH 7.5), 400 mM NaCl, 5% (v/v) glycerol, 10 mM β-mercaptoethanol, 40 mM imidazole) and eluted with buffer containing 200 mM imidazole. The protein buffer was exchanged to 20 mM Tris-HCl (pH 7.5), 200 mM NaCl, 5% (v/v) glycerol, and 5 mM dithiothreitol and concentrated by ultrafiltration to 20 mg ml^{-1}. The molecular mass measured by ESI-MS showed that the N-terminal methionine had been removed.

Dynamic light scattering measurements were performed using a DynaPro plate reader (Protein Solutions, Charlottesville, VA) at room temperature. Molecular weight was also estimated by size-exclusion chromatography on a Sephadex G-75 HR10/30 column. One-dimensional ^1H NMR spectra for mutant and wild-type enzymes were recorded on a Bruker DXR 500-MHz spectrometer and compared with wild-type enzyme to ensure proper folding of the mutant protein.

Crystallization—HisB-N was screened using Hampton solutions (Hampton Research, Aliso Viejo, CA). Optimization of initial hits led to two conditions producing well diffracting crystals: (*a*) 25% (w/v) polyethylene glycol 3350, 0.2 M $MgCl_2$ and 0.1 M Tris-HCl (pH 8.5) by the sitting drop vapor diffusion, and (b) 30% (w/v) polyethylene glycol monomethyl ether, 0.05 M $CaCl_2$, and 0.1 M Bis-Tris (pH 6.5) by the micro-batch method. Both conditions led to isomorphous crystals, space group $C222_1$ with cell dimensions $a = 53.5$, $b = 132.6$, and $c = 107.3$ Å ($Z = 16$) and a V_m of 2.3 $Å^3$ Da^{-1} with 47% solvent content (23).

For structure determination a native crystal grown in the presence of $MgCl_2$ was soaked for 1 min in 1 M NaBr and flash-cooled in the N_2 cold stream (Oxford Cryosystem, Oxford, UK). We refer to these crystals as HisB-N·Mg. The crystals obtained from condition *b* are referred to as HisB-N·Ca. We next soaked crystals obtained from condition *a* in 50 mM histidinol phosphate for 4 h or 50 mM histidinol (product) for 16 h. In both cases only histidinol was observed in the electron density map (HisB-N·Mg/histidinol). Soaking a crystal grown in condition *b* in 50 mM histidinol phosphate for 20 min resulted in the phosphoaspartate complex (HisB-N·Ca/pAsp), and the crystals from *a* were soaked in 0.2 M $MgSO_4$ for 16 h (HisB-N·Mg/sulfate).

Data Collection and Refinement—Data collection for the Br^- SAD experiment was carried out at a wavelength of 0.9202 Å, and the remaining data were collected at a wavelength of 1.1 Å

TABLE 1
Crystallographic data

Dataset	HisB-N·Mg	HisB-N·Ca	HisB-N·Mg/Histidinol	HisB-N·Ca/pAsp	HisB-N·Mg/sulfate
Space group	$C222_1$	$C222_1$	$C222_1$	$C222_1$	$C222_1$
a **(Å)**	53.3	52.7	53.5	53.0	53.6
b **(Å)**	132.0	131.3	132.7	132.4	132.8
c **(Å)**	106.1	104.9	107.3	105.7	107.2
Z	16	16	16	16	16
Resolution (Å)	50-1.7 (1.76-1.7)	50-2.2 (2.28-2.20)	50-1.8 (1.86-1.80)	50-1.75 (1.81-1.75)	50-1.8 (1.86-1.8)
Wavelength (Å)	0.9202	1.7	1.1	1.1	1.1
Observed *hkl*	331,719[a]	113,817	149,328	189,261	151,817
Unique *hkl*	90,017[a]	34,086	34,717	36,862	34,959
Redundancy	3.7 (3.6)	3.4 (2.2)	4.4 (2.4)	5.2 (4.5)	4.4 (2.5)
Completeness	99.9 (99.9)	95.2 (69.4)	96.8 (81.7)	96.8 (92.0)	97.1 (82.6)
R_{sym} **(%)**[b]	0.072 (0.514)	0.029 (0.049)	0.065 (0.429)	0.070 (0.250)	0.067 (0.343)
$I/\sigma(I)$	11.1 (2.9)	39.8 (19.6)	11.8 (2.1)	17.1 (7.1)	12.3 (2.9)
Refinement statistics					
Resolution (Å)[c]	50-1.7	50-2.2	50-1.8	50-1.75	50-1.8
R_{work} *(#hkl)*[d]	0.187 (39463)	0.170 (17045)	0.183 (32981)	0.178 (34795)	0.178 (33235)
R_{free} *(#hkl)*	0.215 (2084)	0.244 (897)	0.223 (1700)	0.211 (1825)	0.213 (1724)
B-factor (Å)²/# atoms					
Protein	14.8 (2533)	22.7 (2568)	18.8 (2546)	15.7 (2565)	15.6 (2533)
Solvent	25.3 (440)	30.4 (315)	32.1 (481)	28.1 (458)	28.8 (513)
Metal ions	16.3 (12)	24.8 (6)	19.9 (8)	15.1 (5)	15.6 (5)
Ligands			20.7 (10)		26.0 (5)
Ramachandran plot					
Allowed (%)	100	100	100	100	100
Disallowed (%)	0	0	0	0	0
Root mean square deviations					
Bonds (Å)	0.009	0.015	0.011	0.009	0.010
Angles (°)	1.175	1.533	1.220	1.281	1.213
PDB code	2FPR	2FPS	2FPU	2FPW	2FPX

[a] Reflections are for unmerged data.
[b] $R_{sym} = (\Sigma|I_{obs} - I_{avg}|)/\Sigma I_{avg}$.
[c] Refinement was performed using merged data for all reflections.
[d] $R_{work} = (\Sigma|F_{obs} - F_{calc}|)/\Sigma F_{obs}$.

using a Quantum-4 charge-coupled device detector (Area Detector Systems Corp., San Diego, CA), at the X8C beamline, National Synchrotron Light Source, Brookhaven National Laboratory. Data processing and scaling were performed with HKL2000 (24). The seven-site Br^- substructure was determined with SHELXD (25), and phases were derived with SHELXE (26). Solvent flattening with RESOLVE (27) led to phases with a figure-of-merit of 0.81. ARP/wARP (28) automatically built 95% of the expected residues. The model was completed manually using XtalView (29) and refined at 1.7-Å resolution with REFMAC5 (30) using all reflections. Difference electron density maps showed the presence of ions in various datasets, and they were modeled as Na^+, Ca^{2+}, Mg^{2+}, Br^-, or Zn^{2+} according to the observed geometry, coordinating atoms, composition of the mother liquor, and refined *B*-factors. There are two molecules in the asymmetric unit. The final model of HisB-N·Mg contains residues 3–19, 22–116, and 120–164 for subunit A, 4–116 and 120–166 for subunit B, and 440 water molecules. The final R_{work} was 0.187, and R_{free} was 0.215 (Table 1). The model has good stereochemistry as analyzed with PROCHECK (31).

Other structures were isomorphous to the native crystals and were refined, starting from the HisB-N·Mg model, at resolutions ranging from 1.75 to 2.2 Å. The metal ions were modeled based on the content of the mother liquor. The R_{work} was ~0.18 and R_{free} was ~0.22 (Table 1). Residues 19–22 and 117–120 were less well defined in the electron density maps and were modeled only in some molecules. The N-terminal His tag was disordered in all crystals.

HPase Assay and Steady-state Kinetics—The HPase assay was carried out as described (32) with release of inorganic phosphate detected as a malachite green·phosphomolybdate complex (33). Each 100-μl reaction mixture contained 25 mM Tris-HCl (pH 7.5), 70 nM enzyme, 25 μM Mg^{2+}, and 200 μM histidinol phosphate. After 15-min incubation at room temperature the reaction was stopped by the addition of 20 μl of molybdate reagent (1.75% (w/v) ammonium heptamolybdate in 6.3 N sulfuric acid). A volume of 20 μl of 0.035% (w/v) malachite green in 0.35% (w/v) polyvinyl alcohol (M_r 14000) in water was added after a 10-min incubation for color development. The absorbance of the malachite green·phosphate complex was recorded at 610 nm after 30 min. A molar absorption coefficient of 110,620 M^{-1} was used to determine the concentration of phosphate released. Values for K_m and k_{cat} were derived through non-linear regression analysis of the Michaelis-Menten equation using duplicate measurements. Eleven different substrate concentrations (10–110 μM) were used for each set of experiments. A reaction time course was also monitored by incubating 10 μM enzyme (native and mutants) with 2–4 mM histidinol phosphate and 5 mM $MgCl_2/CaCl_2$. 3-μl aliquots were withdrawn at various time points for phosphate estimation.

Mass Spectrometric Analysis—Formation of the phosphoaspartate intermediate of HisB-N was followed by ESI-MS using

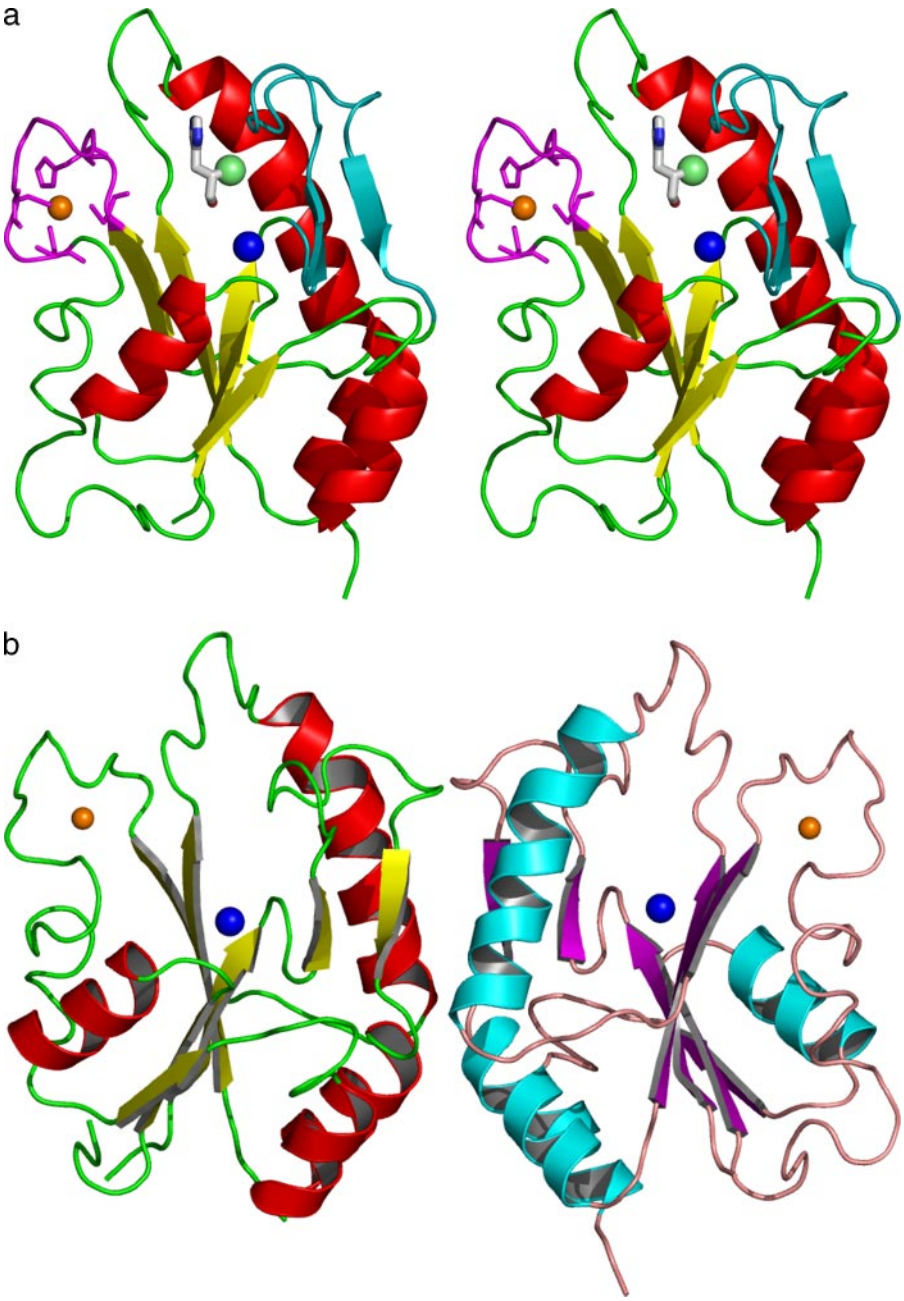

FIGURE 1. *a*, stereo view of the HisB-N monomer with bound histidinol. Secondary structure elements are colored *yellow* and *red*. The Zn^{2+}(*orange*)-stabilized loop is colored *magenta*, and the Ω loop (amino acids 12–34) is colored *cyan*. The Mg^{2+}/Ca^{2+} site 1 is colored *blue*, the site 2 is *green*. The amino group of histidinol occupies site 2. *b*, HisB-N dimer. Subunits are colored differently according to secondary structure elements. The graphics were prepared with the program PyMol (www.pymol.org).

an Agilent 1100 Series LC/MSD (Agilent Technologies, Palo Alto, CA). A 50-μl reaction mixture containing 1 mM histidinol phosphate, 5 mM $MgCl_2$ or $CaCl_2$, and 50 μM HisB-N was incubated at 21 °C for 30 min. A 2-μl aliquot of the reaction mixture was injected directly at 5-min intervals, and the appearance of the phosphoaspartate enzyme adduct was monitored in the positive mode using isocratic conditions of 30% (v/v) acetonitrile containing 0.1% (v/v) formic acid.

Extended X-ray Absorption Fine Structure Measurements—The extended x-ray absorption fine structure spectra for HisB-N were collected at beamline X9B at the National Synchrotron Light Source using a double crystal silicon (111) monochromator. High order harmonics were suppressed (<0.1%) by a nickel-coated reflecting mirror. Data were collected in fluorescent mode using a 13-element Ge array detector (Canberra). All measurements were made with the HisB-N samples in 20 mM Tris-HCl (pH 7.5), 0.2 M NaCl, 5% (v/v) glycerol, and 5 mM dithiothreitol at a protein concentration of 20 mg ml^{-1} in an He-displex cryostat operating at 20 K. Several scans of 40–60 min each were collected and summed together.

Isothermal Titration Calorimetry—ITC measurements were carried out on a MicroCal VP-ITC titration calorimeter (MicroCal, Inc., Northampton, MA) using the VPViewer software for data acquisition and instrument control. Chelex-treated buffer solution (25 mM Tris-HCl, pH 7.0) was used for the metal binding studies, and stocks of metal solutions were prepared using the same buffer. Protein samples treated with 5 mM EDTA for 30 min were chromatographed on a Superose-12 16/60 column with Chelex-treated buffer to remove any bound metal ions. All solutions were degassed prior to the experiment. In a typical experiment HisB-N at a concentration of 260 μM was added to the reaction cell, maintained at 20 °C, and stirred at a constant rate of 260 rpm to ensure rapid mixing. A solution of 5 mM $MgCl_2$ or $CaCl_2$ was loaded into a 300-μl syringe, and 45 injections of 6 μl each were added to the protein sample in 5-min intervals. Data were analyzed using the MicroCal ORIGIN (version 7.0) software provided by the manufacturer. The thermodynamic values K_d, ΔS_o, and ΔH_o for a two-site model were obtained by non-linear curve fitting.

RESULTS AND DISCUSSION

Molecular Structure—The two HisB-N monomers in the asymmetric unit can be superposed with a root mean square deviation of ~0.35 Å for 155 Cα atoms, indicating that no significant conformational differences exist between them. Each monomer has approximate dimensions of 47 × 34 × 26 $Å^3$ and constitutes a single domain containing a Rossmann fold (Fig. 1*a*). The central part of the monomer is formed by a five-stranded parallel β-sheet (β5-β4-β1-β2-β3) flanked on one side by three

α-helices nearly parallel to the β-strands and on the other side by one α-helix and a random coil region resembling a distorted helix (between β3 and β4) (Fig. 1*a*). A long Ω loop (Asp^{12}–Glu^{34}) spans strand β1 and helix α1 and narrows at the ends due to hydrogen bonds between two short β-strands (β1a: Leu^{15}–Ser^{17} and β1b: Ala^{32}–Glu^{34}).

The crystal structure together with dynamic light scattering and size-exclusion chromatography indicate a dimeric organization of HisB-N (Fig. 1*b*). The monomers pack back-to-back via helix α1 (residues Phe^{28}–Leu^{42}) and helix α2 (Leu^{76}–Gln^{84}) to form the dimer with dimensions of ~47 × 68 × 26 $Å^3$. Dimerization mainly involves hydrophobic interactions, with only eight direct hydrogen bonds. Water-mediated hydrogen bonds are observed at the periphery of the dimer interface. The total surface area buried upon dimer formation is ~1250 $Å^2$ corresponding to ~8% of the monomer surface. The substrate-binding site is located on the protein side opposite to the dimerization interface.

Metal Binding Sites—Difference electron density maps calculated from datasets collected for various HisB-N crystals showed the presence of two or three strong peaks (>8σ) near each molecule. Based on the presence of Ca^{2+}, Mg^{2+}, or both Mg^{2+} and Na^+ as well as the observed ligand coordination, these sites were modeled as metal ions (Fig. 1).

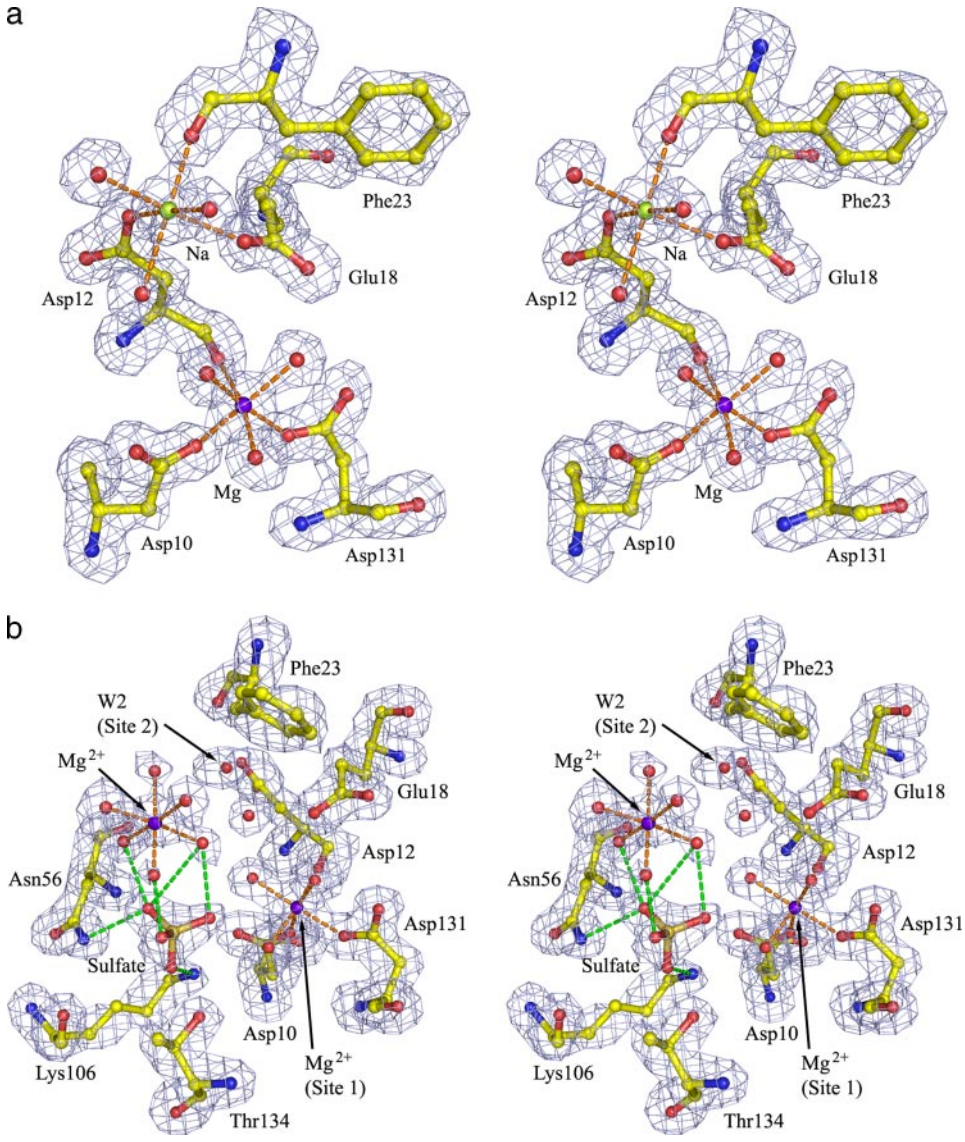

FIGURE 2. *a*, the omit $F_o - F_c$ electron density map for HisB-N·Mg contoured at 3σ. The residues depicted were excluded from the phase calculation. Mg^{2+} occupies site 1 and Na^+ occupies site 2; *b*, the omit $F_o - F_c$ electron density map for HisB-N·Mg/sulfate contoured at 3σ. The depicted residues were excluded from phase calculation. Mg^{2+} occupies site 1, water W2 occupies site 2, a hexa-hydrated Mg^{2+} ion is near the protein surface; *c*, hydrogen bonding interactions within the active site of HisB-N. The HisB-N forms a complex with histidinol. Site 1 is occupied by Mg^{2+}, and site 2 by the amino group of histidinol with its hydroxyl group occupying the position of water W1; *d*, the HisB-N·phosphoaspartate intermediate.

Zinc Binding Site—The Zn^{2+} ion is present in all HisB-N molecules. Its presence was confirmed by extended x-ray absorption fine structure analysis, which showed strong absorption at the K edge of zinc (9668 eV, data not shown). This site is situated within the loop following strand β5. The side chains of Cys^{94}, His^{96}, Cys^{102}, and Cys^{104} tetrahedrally coordinate the Zn^{2+}. The average Zn^{2+} distance to the cysteine thiol groups is 2.3 Å and to $ND1^{His\text{-}96}$ is 2.1 Å (Fig. 1*a*). The temperature factor for this Zn^{2+}, (~16 $Å^2$), is similar to the average B-factor of the surrounding protein atoms. Since Zn^{2+} was not part of the crystallization conditions, its presence in the crystal structure indicates that HisB-N acquired Zn^{2+} during expression in *E. coli* and that this metal is required for maintaining the structural integrity of the protein. The Zn^{2+} site is ~14 Å away from the catalytic Asp^{10}.

Metal Site 1—HisB-N·Mg crystals show a metal-binding site near the active site Asp^{10} coordinated by six O atoms with octahedral geometry (Fig. 2*a*). The average metal-O distance of 2.1 Å confirms the presence of Mg^{2+}. This site is common to both monomers and is situated above strands β1 and β4. The Mg^{2+} is coordinated by the side-chain oxygens $O\delta2^{Asp\text{-}10}$ and $O\delta1^{Asp\text{-}131}$, the main-chain oxygen $O^{Asp\text{-}12}$, and three water molecules. In crystals of HisB-N·Ca grown in the presence of 50 mM $CaCl_2$, this site is occupied by a Ca^{2+} and is coordinated by the same residues as described for the Mg^{2+} site, except that the average Ca^{2+}-O distance is 2.35 Å.

Metal Site 2—In the HisB-N·Ca/pAsp complex there is a second metal ion with octahedral coordination (in molecule B only) ~6 Å away from site 1. This site is located between strands β2 and β4. The metal ion is coordinated by $O\delta2^{Asp\text{-}12}$, $O^{Phe\text{-}23}$, and four water molecules. The average ion-O distance is 2.35 Å, indicative of Ca^{2+}.

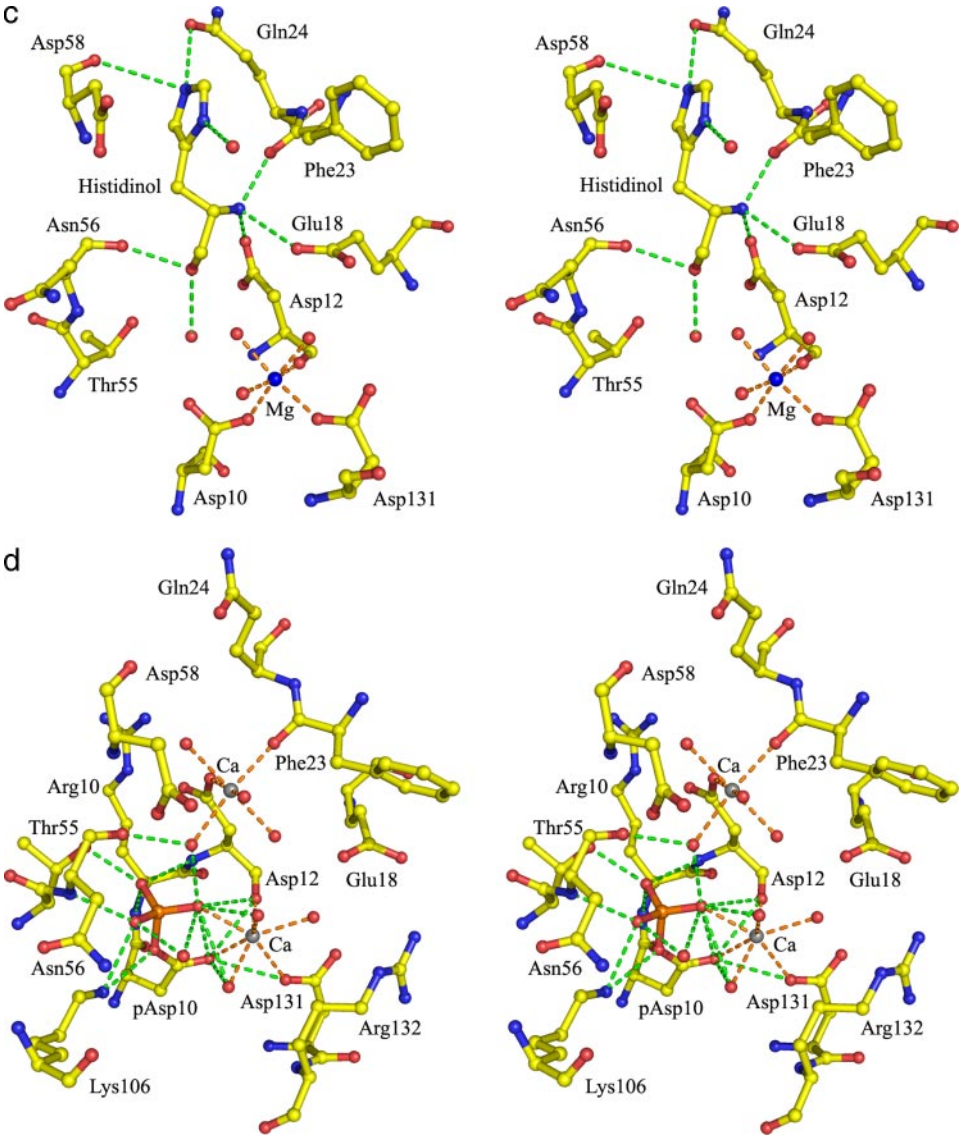

FIGURE 2—*continued*

TABLE 2
Binding constants of metals by ITC for the wild-type HisB-N

Metal	K_d	ΔH_0	ΔS_0
	μM	kcal·mol^{-1}	cal·mol^{-1}·K^{-1}
Mg^{2+}			
Site 1	0.10 ± 0.04	−3.20 ± 0.05	21.1
Site 2	3.10 ± 0.48	−0.64 ± 0.04	23.0
Ca^{2+}			
Site 1	0.08 ± 0.01	−4.20 ± 0.09	18.1
Site 2	5.68 ± 1.07	−0.89 ± 0.03	21.0

This site is also occupied in the crystal of HisB-N·Mg soaked briefly in 1 M NaBr. In this case, the $OE2^{Glu\text{-}18}$ atom replaces one of the water molecules in the coordination sphere (Fig. 2*a*) with an average ion-oxygen distance of 2.45 Å, substantially longer than that expected for Mg^{2+}-O but in accordance with the distance expected for Na^{+}-O coordination.

In crystals grown from $CaCl_2$ (HisB-N·Ca) or soaked with $MgSO_4$ (HisB-N·Mg/sulfate) a tetrahedrally coordinated water molecule occupies this site (Fig. 2*b*). In the latter structure we observe a fully hydrated Mg^{2+} ion (octahedral coordination by six water molecules, average distance 2.1 Å) ~5 Å from site 2 and near the protein surface. This cluster is hydrogen-bonded to the side chains of Arg^{132}, Arg^{105}, and Asp^{58} and to the sulfate ion.

ITC Measurements of Metal Binding Affinities—We measured binding of Mg^{2+} and Ca^{2+} to HisB-N by ITC. Titration of HisB-N in the absence of substrate with either Mg^{2+} or Ca^{2+} confirmed the presence of two metal-binding sites with binding constants differing ~50-fold (Table 2). Based on the crystal structures, site 1 is likely the primary site with ~100 nM affinity for the first Mg^{2+} and site 2 is the secondary site with an affinity of ~3 μM. The affinity for the first Ca^{2+} ion is 77 nM and ~6 μM for the second. The relatively low affinity of site 2 concurs with our finding that in apo-HisB-N at low Ca^{2+} concentration a water molecule occupies this site. Furthermore, the presence of Ca^{2+} in site 2 in HisB-N·Ca/pAsp but not in HisB-N·Ca at an identical Ca^{2+} concentration indicates that the affinity of site 2 is enhanced upon formation of the phosphoaspartate intermediate.

HisB-N·Histidinol Complex—The difference Fourier map for crystals of HisB-N soaked with either histidinol phosphate or histidinol in the presence of Mg^{2+} showed identical electron density in the substrate-binding site of molecule B consistent with the histidinol moiety, thus indicating retention of enzymatic activity in the crystal. No density for histidinol was observed in molecule A, because this site is blocked by the Arg^{165} side chain from a neighboring molecule.

The histidinol is positioned within the cleft formed at the top of the central β-sheet over strand β1 (Fig. 1). Its imidazole ring stacks against the flat face of the Asp^{58} side chain on one side and against the backbone and Cβ atoms of Phe^{23} on the other side. The ring also makes herring bone interactions with Phe^{65}. Histidinol forms five direct hydrogen bonds to the protein: Nϵ2 . . . $O\epsilon1^{Gln\text{-}24}$, N . . . $O\epsilon2^{Glu\text{-}18}$, N . . . $O^{Phe\text{-}23}$, N . . . $O\delta2^{Asp\text{-}12}$, O(H) . . . $O^{Asn\text{-}56}$, and several additional water-mediated H-bonds (Fig. 2*c*). One of these waters is within the coordination sphere of the Mg^{2+} ion. The amino group of the histidinol displaces the metal in site 2, whereas its hydroxyl O(H) displaces a water molecule observed in the active site in other HisB-N ligand complexes.

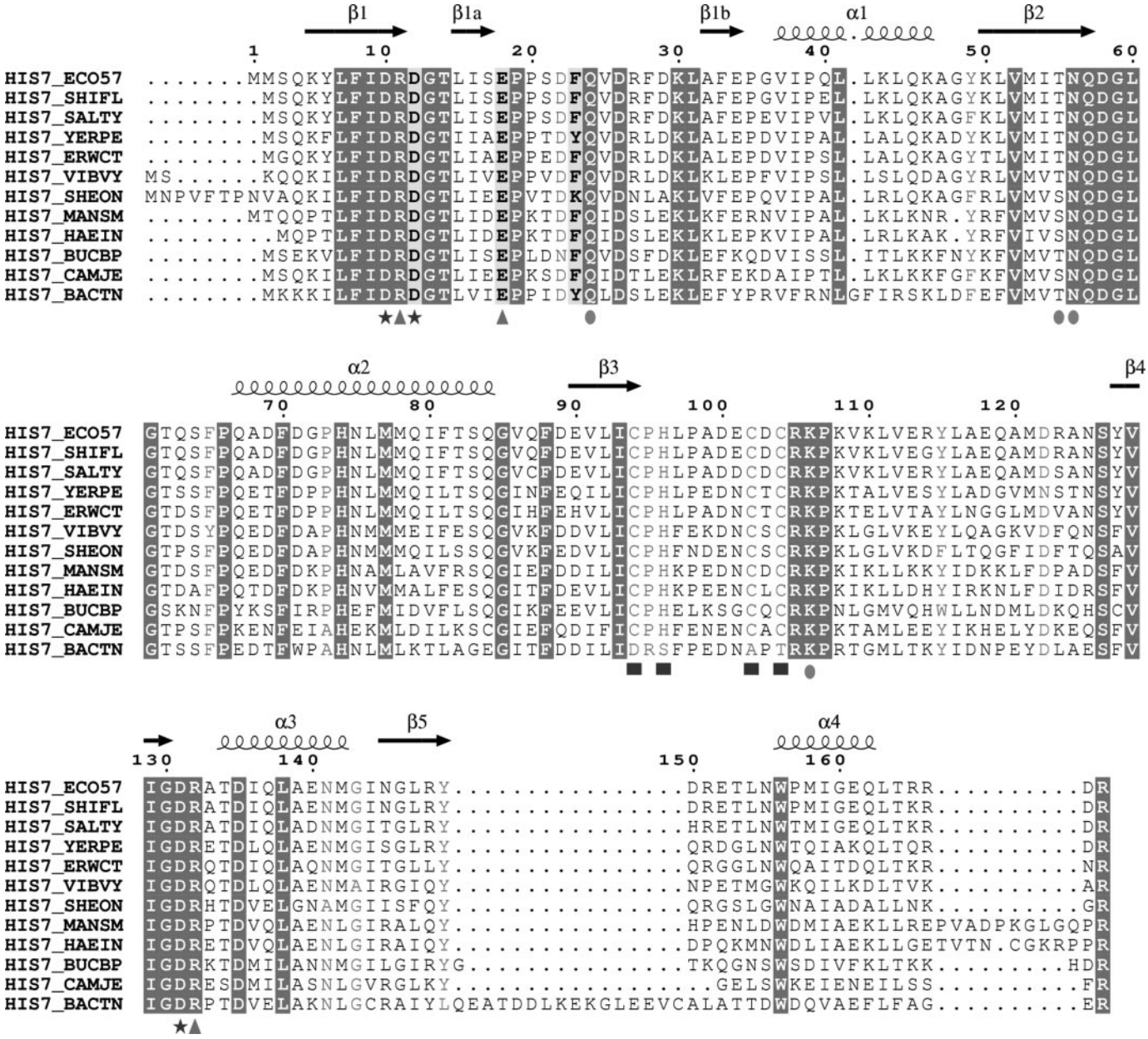

FIGURE 3. **Sequence comparison of the N-terminal domain of bifunctional HisB enzymes.** Strictly conserved residues are shown in black on *gray* background with semi-conserved residues represented by *white letters* on dark background. Residues involved in metal binding are marked by an *asterisk*. Core catalytic residues are marked by *circles*, and Zn^{2+}-binding sites are marked by *squares*.

Phosphoaspartate Intermediate—The dephosphorylation of substrates catalyzed by enzymes from the HAD superfamily takes place through the formation of a covalent phosphoaspartate intermediate (13–16, 18). This intermediate was trapped in HisB-N·Ca/pAsp when a crystal was soaked in histidinol phosphate in the presence of Ca^{2+}. The difference electron density clearly showed the covalent attachment of a phosphoryl group to the side chain of Asp^{10}. This phosphoryl group participates in an extensive hydrogen-bonding network to the main chain of Arg^{11}, Asp^{12}, and Asn^{56} and to the side chains of Lys^{106} and Thr^{55}. The terminal OP1 oxygen atom participates in the coordination sphere of Ca^{2+} in site 1 leading to some rearrangement of waters and a change in Ca^{2+} coordination from hexadentate to heptadentate (average Ca^{2+}-O distance of 2.40 Å, Fig. 2*d*). Simultaneously, the side chain of Arg^{132} rotates outward creating a wider opening of the substrate binding site.

Sulfate Binding Site—In the crystal structure of HisB-N·Mg/sulfate, obtained by soaking a native crystal in 200 mM $MgSO_4$, we observed one sulfate ion in the substrate-binding cleft. This ion was found in the upper part of the cleft, ~5 Å above the catalytic Asp^{10}, close to the protein surface. The sulfate is hydrogen-bonded to the side chains of Gln^{56}, Lys^{106}, and Thr^{134} and to the hydrated Mg^{2+} cluster near the protein surface (Fig. 2*b*). The side chain of Lys^{106} adopts a slightly different orientation from that observed in the HisB-N·Ca/pAsp complex. We propose that the position of this sulfate ion delineates the exit route of the phosphate following release from Asp^{10}. The tight binding of the sulfate to the hexahydrated Mg^{2+} via hydrogen bonds suggests that the Mg^{2+} plays a role in phosphate release.

Sequence and Structural Comparisons—The *E. coli* HisB-N domain has counterparts in many bacteria, with sequences for over 220 HPases presently known. This protein family belongs to the very large haloacid dehalogenase-like (HAD) superfamily, which includes more than 6000 proteins (PFAM, PF00702). Specifically, HisB-N belongs to the HAD IIIA subfamily of aspartate-nucleophile hydrolases that are characterized by the lack of a "cap domain" over the substrate-binding site (34). The HAD superfamily is distinguished by the presence of an N-terminal motif containing the aspartate nucleophile, a central motif containing a conserved lysine (or arginine) and a C-terminal motif containing a conserved serine/threonine and aspartate (11) (Fig. 3). In HisB-N these residues are Asp^{10}, Lys^{106}, and Asp^{131}, respectively. The sequences of proteins annotated as HPases or histidinol phosphatase-related show additional absolutely conserved residues, corresponding in HisB to Arg^{11}, Asp^{12}, Ser/Thr^{55}, Asn^{56}, Gln^{57}, Arg^{105}, Pro^{107}, and Gly^{130}. The Cys^{94}-*X*-His-$(X)_5$-Cys-*X*-Cys^{104} motif forming the Zn^{2+}-binding site (Fig. 1*a*) is present in the majority of these proteins, suggesting that most of them require stabilization by Zn^{2+}. In addition, Glu^{18}, Gln^{24}, Asp^{58}, and Arg^{132} are present in all bifunctional HPases but not in some histidinol phosphatase-related proteins. Their conservation in only the HPases suggests a role in defining substrate specificity.

The closest structural homologs of HisB-N are the phosphatase domain of mouse 5′-polynucleotide kinase-3′ phosphatase (PDB code 1YJ5 (35)), mouse magnesium-dependent phosphatase-1 (PDB code 1U7P (36)), and acid phosphatase (AphA) from *E. coli* (PDB code 1N8N (37)). Enzymes from subfamily III often form oligomers where the substrate-binding site of one subunit is partially occluded by another subunit (PDB 1J8D (38)). In other cases, such as *E. coli* AphA, the substrate-binding site is more open, accounting for the observed lack of specificity of this enzyme. HisB-N employs an Ω loop following strand β1 (in particular Phe^{23} and Asp^{58}–Phe^{65}) and the Zn^{2+}-binding loop (Cys^{94}–Lys^{106}) to create a deep and narrow substrate binding site for accommodating histidinol phosphate. The Mg^{2+} observed in other HAD enzymes is also present in HisB-N at site 1 and is coordinated by the conserved residues Asp^{10}, Asp^{12}, and Asp^{131}. The metal ion observed in site 2, near the catalytic site, is unique to HisB-N and has not been observed in other HAD enzymes.

Mutagenesis of Asp^{12} and Glu^{18}—Asp^{12} and Glu^{18} were mutated to alanine or serine to determine their potential as water-activating nucleophiles. The Asp^{12} → Ala, Asp^{12} → Ser, Glu^{18} → Ala, and Glu^{18} → Ser mutants showed similar elution profiles as wild-type protein by gel-filtration chromatography, and the alanine mutants showed ^1H NMR spectra characteristic for folded proteins. Under our standard assay conditions these mutants showed no measurable activity.

To measure residual HPase activity we repeated the assay at 140-fold higher protein concentration (10 μM) and longer incubation times. Under these conditions, the Glu^{18} → Ala mutant showed ~5% of the wild-type activity (Fig. 4) indicating that Glu^{18}, while important, is dispensable. This side chain participates in the coordination of a metal ion at site 2, and its mutation would be expected to weaken metal binding. Increasing the concentration of Mg^{2+} from 5 μM to 1 mM led to a dramatic increase of activity of this mutant (Fig. 4*b*), suggesting that Mg^{2+} at site 2 is essential for catalysis.

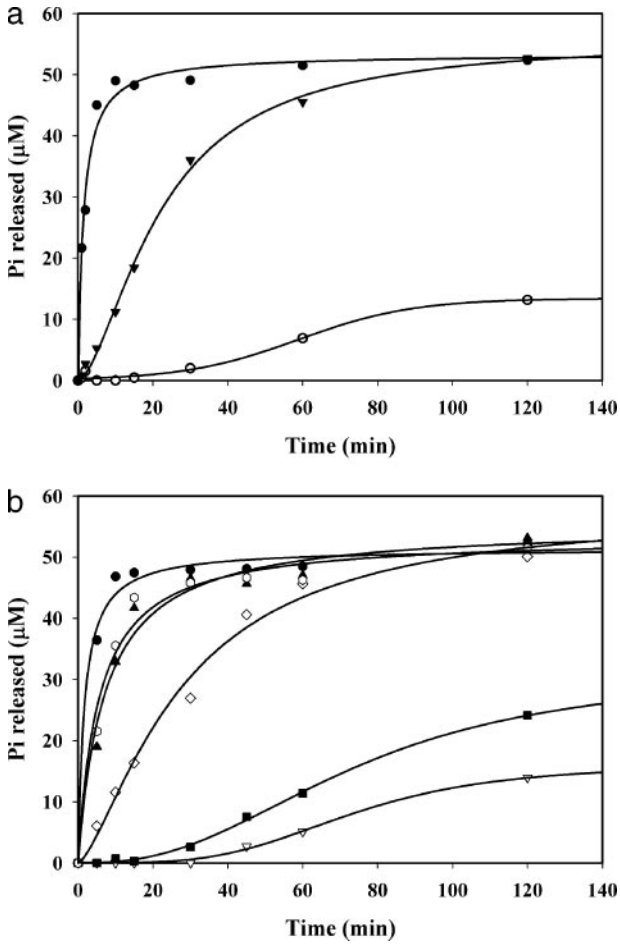

FIGURE 4. **HPase activity of wild-type and mutant HisB-N.** *a*, activity of HisB-N (200 nM) in the presence of 5 mM $MgCl_2$ (●), $CaCl_2$ (○), and HisB-N·Glu^{18}Ala (10 μM) in the presence of 5 mM $MgCl_2$ (▼). *b*, activity of HisB-N (200 nM) in the presence of 5 μM $MgCl_2$ (●) and HisB-N·Glu^{18}Ala (10 μM) in the presence of 5 μM (▽), 10 μM (■), 100 μM (◇), 1 mM (▲), and 5 mM (○) $MgCl_2$.

Conversely, the Asp^{12} → Ala mutant showed only traces of activity, even with overnight incubation in the presence of 1 mM Mg^{2+}, showing that the presence of the Asp^{12} side chain is essential for enzyme activity. When assayed in the presence of Ca^{2+} neither the Glu^{18} → Ala nor the Asp^{12} → Ala mutant showed any detectable activity.

Mechanism of Action—The various structures we have determined represent snapshots along the HisB-N reaction pathway (Fig. 5*a*). The HisB-N·Mg model (see "Experimental Procedures") shows the initial state of the enzyme. In the resting state, a water molecule (W2) rather than a Na^+ ion occupies site 2, as observed in the HisB-N·Ca structure. Two other key sites within the active site are occupied by water molecules (W1 and W3) in the HisB-N·Mg and HisB-N·Ca structures. We have modeled histidinol phosphate bound to HisB-N based on the HisB-N·histidinol and HisB-N·Ca/pAsp structures. Substrate binding displaces these waters, with W1 replaced by the histidinol hydroxyl, W2 by the histidinol amino group, and W3 by the phosphate oxygen (Fig. 5*a*). This orientation of the substrate presents its phosphoryl group for nucleophilic attack by the side chain of Asp^{10}. The reaction proceeds through a penta-

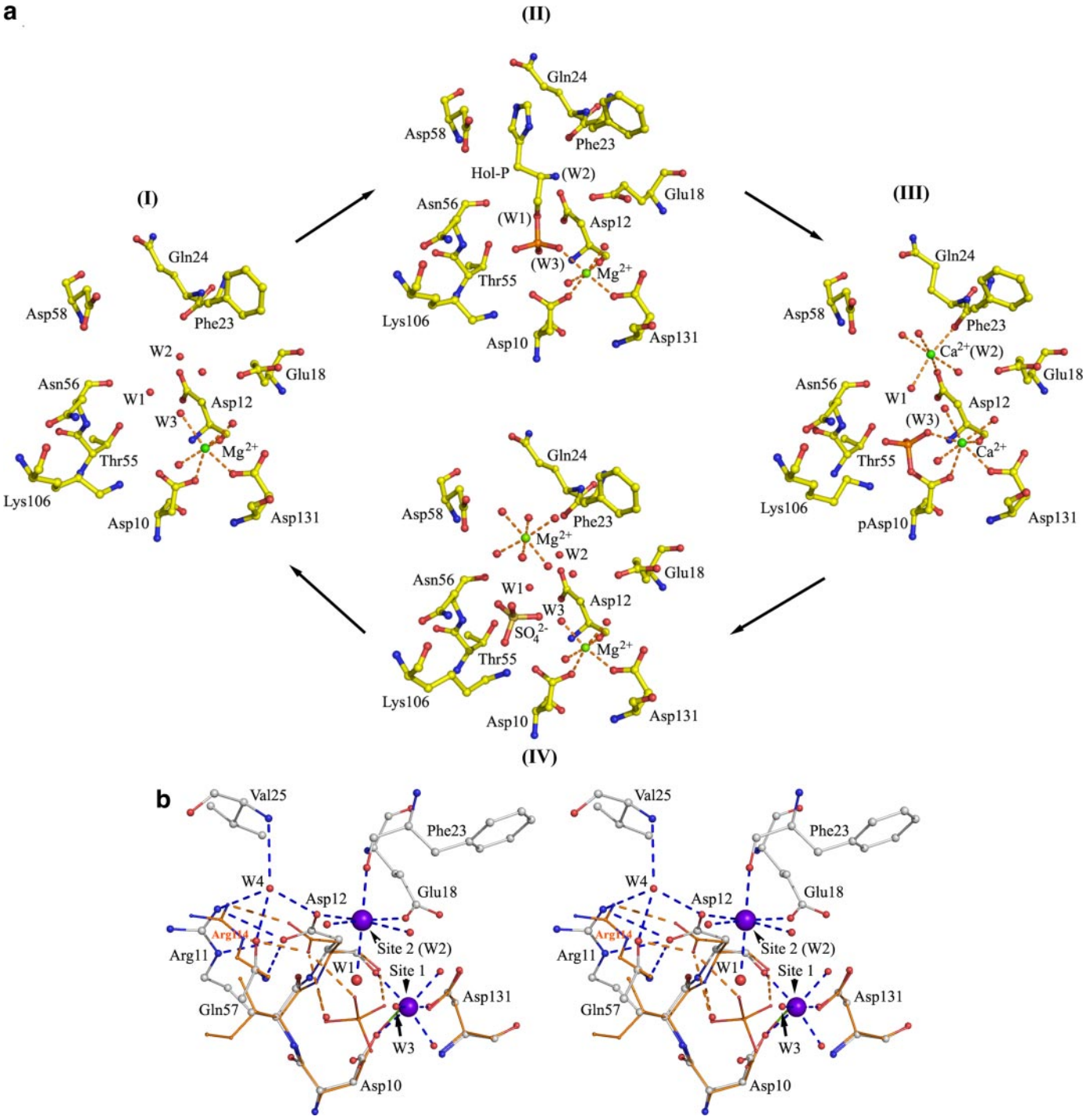

FIGURE 5. *a*, states along the reaction pathway based on determined structures. *I*, the initial state with site 1 occupied by Mg^{2+}; *II*, HisB-N with histidinol phosphate substrate modeled on the structure of histidinol complex; *III*, phosphoaspartate intermediate with Mg^{2+} occupying sites 1 and 2; *IV*, release of phosphate and Mg^{2+} from site 2; *b*, superposition of the active site residues of HisB-N (gray) with *E. coli* AphA (*orange*). *Red spheres* represent water molecules; *violet spheres* show metal binding sites. The orientations of Asp^{12} and its equivalent in AphA are different. Asp^{12} is stabilized by hydrogen bonds (*blue*) to Arg^{11}, site 2, and bridging water W4. Asp^{46} of AphA is hydrogen-bonded (*orange*) to Arg^{114}, approaching from the opposite direction to Arg^{11} of HisB-N, and to the of phosphate oxygen in the position of water W1. Only HisB residues are labeled.

valent transition state (14, 17) resulting in a covalent phosphoaspartate intermediate with an inversion of configuration of the phosphorus, and release of histidinol. Direct coordination of the metal in site 1 to the phosphoryl group neutralizes its negative charge and stabilizes the covalent intermediate. Additional stabilization of the phosphoryl group is provided by the side chain of Lys^{106}, the backbone NH of Asp^{12} and Asn^{56}, and bridging water molecules (Fig. 5*a*). The HisB-N·Ca/pAsp structure provides direct evidence for the formation of a phosphoaspartate intermediate in the reaction catalyzed by HPase and also shows that the release of histidinol after the formation of phosphoaspartate facilitates binding of the second metal at site

2. A similar phosphoaspartate intermediate was previously observed in the structure of β-phosphoglucomutase (18). The second step, hydrolysis of the phosphoaspartate, is performed by a water molecule W1, which occupies the position of the histidinol hydroxyl group in the substrate, and is within the coordination sphere of the metal in site 2.

The presently known structures of HAD phosphohydrolases/phosphotransferases suggest that the aspartate (Asp^{12} in HisB) positioned two residues after the catalytic aspartate (Asp^{10} in HisB) acts as a general acid donating proton to the leaving group (15). The same aspartate is presumed to play the role of general base in the second half-reaction, activating the water molecule W1. This aspartate is directed toward the position occupied either by the oxygen of the scissile P–O bond in the substrate (enzyme·substrate complex) and, hence, is in a position to protonate the leaving group, or by water W1 (phosphoaspartate intermediate) ready for inline attack on the phosphoaspartate (Fig. 5*b*). In AphA from *E. coli* (37) and sugar phosphatase from *Bacteroides thetaiotaomicron* (39) this orientation of the aspartate side chain is stabilized through a salt bridge to an arginine. However, in HisB-N the carboxylate of Asp^{12} is rotated by ~70° away from the crucial water W1 and is directed toward site 2 (Fig. 5*b*). Furthermore, this orientation of Asp^{12} is stabilized by a salt bridge to Arg^{11} ($NE^{Arg\text{-}11}$ . . . $O\delta1^{Asp\text{-}12}$ . . . $NH_2^{Arg\text{-}11}$, conserved in HPases but distinct from other HAD enzymes), by a hydrogen bond to a bridging water W4 (present in all HisB-N structures), and the interactions with the water W2 or metal occupying site 2 (Fig. 5*b*). These structural restrictions confine the orientation of Asp^{12} away from W1 and put into question the ability of Asp^{12} to act as a general acid protonating histidinol and a general base activating water W1. Mutation of Asp^{12} to an alanine or a serine leads to an inactive enzyme, however, this may reflect a destabilization of the active/substrate binding site, because these mutants express poorly and could not be crystallized even when micro-seeded with crystals of the native enzyme. This behavior suggests that Asp^{12} is essential for the integrity of both the active and substrate-binding sites and could play an indirect rather that direct role in the enzymatic mechanism. If this is indeed the case, it is unclear where the proton required for histidinol protonation comes from.

TABLE 3
Effect of metals on wild-type HPase activity

Metal	k_{cat}	K_m	k_{cat}/K_m
50 μM	$\times 10^3\ s^{-1}$	*μM*	$\times 10^8\ s^{-1}\ M^{-1}$
Co^{2+}	2.05 ± 0.10	54 ± 6	3.81
Mg^{2+}	2.14 ± 0.09	54 ± 5	3.96
Zn^{2+}	1.41 ± 0.07	41 ± 5	2.61
Mn^{2+}	0.96 ± 0.04	52 ± 5	1.78
Ca^{2+}	NM[a]	NM	

[a] NM, not measurable.

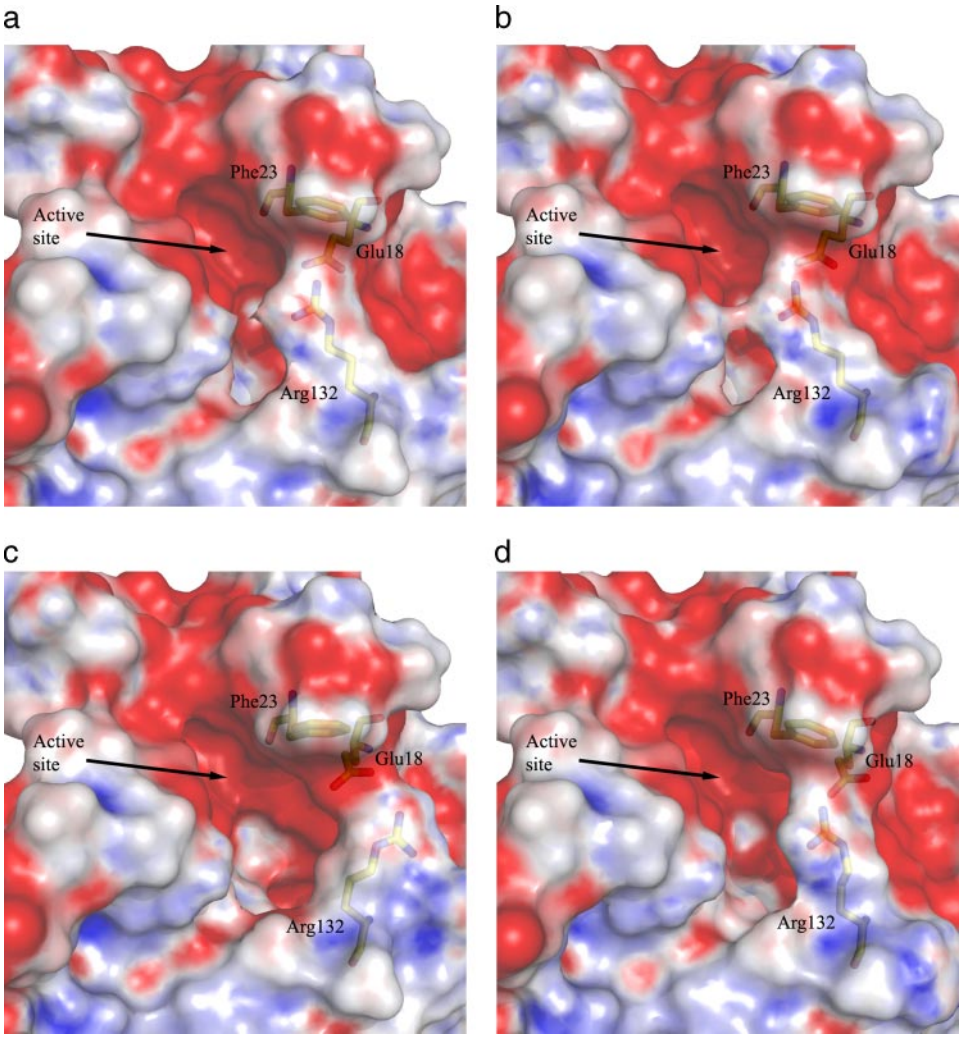

FIGURE 6. **Changes in the HisB-N substrate binding region along the reaction pathway shown in a surface representation.** The residues that undergo conformational changes due to binding of the substrate and/or metal ions, namely Glu^{18}, Phe^{23}, and Arg^{132} are shown as *sticks* under semitransparent surface. All structures are shown in the same orientation. *a*, HisB-N·Mg; *b*, HisB-N·Mg/histidinol; *c*, HisB-N·Ca/pAsp; and *d*, HisB-N·Mg/sulfate.

We propose that in HisB-N, the metal ion at site 2 (usually Mg^{2+}) is essential for the second half-reaction by assisting in the deprotonation of water W1 (its ligand), possibly by aiding Asp^{12}, whose Oδ1 atom is adjacent to water W1 in the octahedral coordination environment (Fig. 5). Water W1 also forms a hydrogen bond to $O^{Asn\text{-}56}$. The latter interaction likely helps in proper positioning of water W1 for nucleophilic attack on the phosphoaspartate. The importance of the metal in site 2 is supported by mutations of Gln^{18} that participates in coordination of the metal in site 2. $Gln^{18} \rightarrow$ Ala or $Gln^{18} \rightarrow$ Ser mutation reduces the affinity of site 2 for the

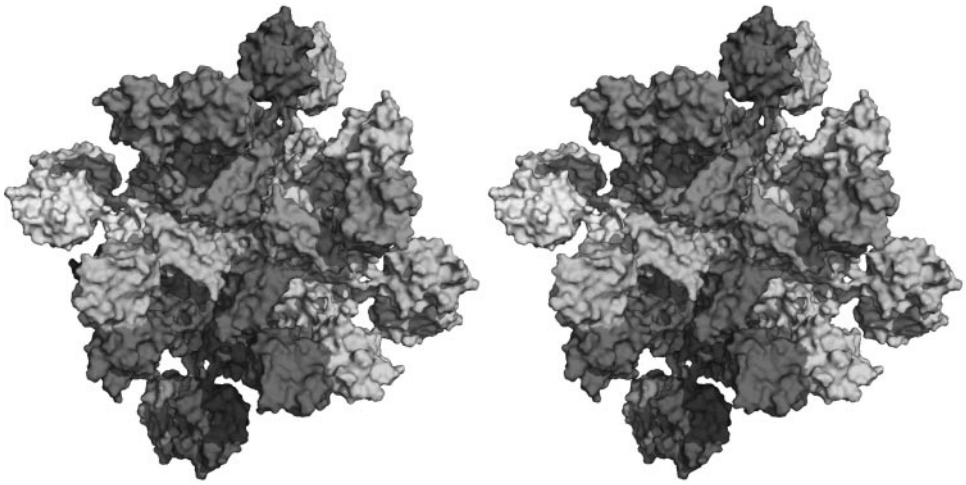

FIGURE 7. **Oligomeric structure of the full-length HisB.** The monomeric units are shaded differently. The model is reconstructed based on the oligomeric models of the monofunctional IGPDs from *F. neoformans* (PDB 1RHY (4)) and *S. aureus* subsp. N315 (PDB 2AE8, unpublished observation), and the dimeric HisB N-terminal domain.

metal, accounting for the observed drastic decrease in enzymatic activity. However, increasing the concentration of Mg^{2+} can restore activity. The structure of HisB-N·Mg/sulfate represents the final reaction step where the sulfate ion mimics the phosphate product guided to the surface by Gln^{56} and Lys^{106} and is accompanied by a fully hydrated hexa-coordinated Mg^{2+} ion departed from site 2. Site 1 remains occupied by the Mg^{2+} ion. The release of phosphate and the metal from site 2 restores the enzyme to its initial state.

The conservation of Glu^{18} and all residues forming metal binding sites in the sequences of all histidinol phosphatases but not other HAD enzymes strongly suggests that the proposed novel mechanistic variant is common to this entire subfamily. This mechanism, in which two-Mg^{2+} ions are employed in catalysis, and the water is activated directly by the metal ion, is highly reminiscent of the mechanism employed by polymerases (exonuclease domain), ribonucleases, and alkaline phosphatase to break the phosphoryl bond in nucleic acids (reviewed in Ref. 40).

Mode of Inhibition by Calcium—HisB-N shows high catalytic efficiency in the presence of metal ions (Table 3). In the presence of 50 μM Mg^{2+} or Co^{2+} the enzyme had similar k_{cat}/K_m ($\sim 3.8 \times 10^8\ s^{-1}\ M^{-1}$), whereas the activities in the presence of Zn^{2+} or Mn^{2+} were 30 and 50% lower, respectively. No enzymatic activity was detected in the presence of either Ca^{2+} or EDTA (100 μM). The effect of EDTA could be reversed by the addition of excess metals. A similar activity profile has been observed for HisB from *Salmonella typhimurium* (9).

The loss of enzymatic activity correlates with an increase in the atomic radius of the metal (calcium being significantly larger than other metals tested), which can be rationalized based on the crystal structure of HisB-N·Ca/pAsp. In the presence of Ca^{2+}, the phosphoaspartate intermediate is trapped in the crystal, indicating that the first half-reaction is unaffected and that inhibition occurs at the second half-reaction. The transfer of the phosphoryl group from histidinol phosphate to Asp^{10} occurs as in the presence of Mg^{2+}, with one oxygen of the phosphoaspartate intermediate coordinating the metal in site 1. However, the larger radius of Ca^{2+} *versus* Mg^{2+} causes a small rearrangement of water molecules, leading to a hepta-coordinated Ca^{2+} (Fig. 2*b*). Consequently, the phosphoryl group is likely shifted by ~1 Å, relative to its position in the presence of a smaller Mg^{2+} ion, and occupies a suboptimal position for nucleophilic attack by water W1. In addition, the Ca^{2+} ion in site 2 also rearranges the coordination sphere compared with a smaller ion (*e.g.* Mg^{2+}). The side chain of Glu^{18} is excluded from the Ca^{2+} coordination sphere and is replaced by a water molecule to which it is hydrogen-bonded. Ca^{2+} has previously been shown to inhibit another HAD enzyme, human phosphoserine phosphatase (41). However, based on the crystal structure, a different mechanism of inhibition was proposed, in which the bidentate coordination of Ca^{2+} to Asp^{20} (equivalent to Asp^{10} in HisB) prevents the aspartate from acting as a nucleophile.

To investigate formation of the phosphoaspartate during catalysis *in vitro* we have followed the reaction by mass spectrometry and detected the phosphoaspartate by ESI-MS during a reaction time course. In the presence of Mg^{2+} and histidinol phosphate only one species with a molecular mass of 19,903 Da was present. This mass corresponds well to the enzyme with the N-terminal methionine removed (theoretical molecular mass is 19,909 Da). In the presence of Ca^{2+} and histidinol phosphate we observed the accumulation of a species (~30% of the wild-type enzyme) with a mass of 19,983 Da, corresponding to that expected for the phosphoaspartate enzyme adduct (+79 Da), consistent with the crystal structure of HisB-N·Ca/pAsp.

Dynamics of the Active Site—Comparison of all the HisB-N molecules provides insight into the dynamics of the substrate-binding cavity at various stages of the histidinol phosphate dephosphorylation reaction (Fig. 6). Two residues show substantial movements that affect the size of the entrance to the active site cleft, namely Arg^{132} and Glu^{18}. In the apo model the active site is relatively open for binding the substrate. Upon binding of the substrate, the side chains of Arg^{132} and Glu^{18} move inward resulting in narrowing the entrance to the binding site and capturing the substrate (Fig. 6*b*). After the first half-reaction, *i.e.* the formation of a phosphoaspartate intermediate, the side chain of Glu^{18} rotates away from the active site and Arg^{132} swings out, resulting in a widening of the cavity and enabling the release of histidinol (Fig. 6*c*). The hydrolysis of phosphoaspartate is accompanied by the restoration of the Arg^{132} side chain to its original position and the release of the phosphate (possibly together with a hydrated Mg^{2+} ion) guided by the side chain of Lys^{105}.

The opening and closing of the active site is not uncommon to enzymes belonging to the HAD superfamily, especially in enzymes containing the cap (sub)domain, although the rearrangement is largely restricted to the cap domain. Similarly

to HisB, bacterial acid phosphatase AphA from *E. coli*, lacking the cap domain, also exhibits the opening and closing of the active site based on the absence or presence of a phosphorylated substrate, through a loop movement representing the "open" and "closed" states (15). Notable examples of domain shifts observed in members possessing the cap domains include phosphoserine phosphatase from *Methanococcus jannaschi* (42) and a phosphatase from *Thermotoga maritima* (43).

Oligomeric State of the Full-length HisB—We asked the question of the organization of the dimeric N-terminal HisB domain in the context of the full-length HisB. The C-terminal IGPD domain of HisB shows ~50% sequence identity to monofunctional IGPDs from *Filobasidiella neoformans* (44) and *Arabidopsis thaliana* (45) both of which form 24-mers in the presence of Mn^{2+}. We have found that in the presence of 5 mM Mn^{2+} HisB also associates into large oligomers that eluted from Sephacryl S-300 gel filtration column near the void volume corresponding to ~900 kDa, and dynamic light scattering showed apparent molecular mass of ~800 kDa. The phosphatase activity of HisB in the presence of Mn^{2+} remained unaltered, indicating that HisB oligomerization has no effect on HisB-N activity. Based on the structure of HisB-N and the structure of corresponding IGPD domains from orthologous protein we constructed a model of the bifunctional HisB in which the IGPD domain is a 24-mer. A unique way of matching the N- and C-terminal domains was apparent (Fig. 7). This model suggests that the basic unit of HisB is a hexamer.

Acknowledgments—We thank Dr. K. Gehring for the use of ITC instrument, V. J. Davisson for providing us with histidinol phosphate, Dr. A. Ignatov for assistance in carrying out extended X-ray absorption fine structure data collection, Dr. I. Ekiel for NMR analysis, Dr. M. McMillan and Dr. A. Soares for assistance in x-ray diffraction data collection, and Dr. T. Sulea for helpful discussions. Data for this study were measured at beamlines X8C, X12B, and X9B of the National Synchrotron Light Source, Brookhaven National Laboratory.

REFERENCES

1. Winkler, M. E. (1996) in *Escherichia coli and Salmonella typhimurium: Cellular and Molecular Biology* (Neidhardt, F. C., ed) pp. 485–505, ASM Press
2. Alifano, P., Fani, R., Lio, P., Lazcano, A., Bazzicalupo, M., Carlomagno, M. S., and Bruni, C. B. (1996) *Microbiol. Rev.* **60,** 44–69
3. Brilli, M., and Fani, R. (2004) *J. Mol. Evol.* **58,** 225–237
4. Chiariotti, L., Nappo, A. G., Carlomagno, M. S., and Bruni, C. B. (1986) *Mol. Gen. Genet.* **202,** 42–47
5. Carlomagno, M. S., Chiariotti, L., Alifano, P., Nappo, A. G., and Bruni, C. B. (1988) *J. Mol. Biol.* **203,** 585–606
6. Loper, J. C. (1961) *Proc. Natl. Acad. Sci. U. S. A.* **47,** 1440–1450
7. Brady, D. R., and Houston, L. L. (1973) *J. Biol. Chem.* **248,** 2588–2592
8. Chumley, F. G., and Roth, J. R. (1981) *J. Mol. Biol.* **145,** 697–712
9. Houston, L. L., and Graham, M. E. (1974) *Arch. Biochem. Biophys.* **162,** 513–522
10. Thaller, M. C., Schippa, S., and Rossolini, G. M. (1998) *Protein Sci.* **7,** 1647–1652
11. Aravind, L., Galperin, M. Y., and Koonin, E. V. (1998) *Trends Biochem. Sci.* **23,** 127–129
12. Allen, K. N., and Dunaway-Mariano, D. (2004) *Trends Biochem. Sci.* **29,** 495–503
13. Collet, J. F., Stroobant, V., Pirard, M., Delpierre, G., and Van, S. E. (1998) *J. Biol. Chem.* **273,** 14107–14112
14. Wang, W., Kim, R., Jancarik, J., Yokota, H., and Kim, S. H. (2001) *Structure* **9,** 65–71
15. Calderone, V., Forleo, C., Benvenuti, M., Thaller, M. C., Rossolini, G. M., and Mangani, S. (2006) *J. Mol. Biol.* **355,** 708–721
16. Rinaldo-Matthis, A., Rampazzo, C., Reichard, P., Bianchi, V., and Nordlund, P. (2002) *Nat. Struct. Biol.* **9,** 779–787
17. Lahiri, S. D., Zhang, G., Dunaway-Mariano, D., and Allen, K. N. (2003) *Science* **299,** 2067–2071
18. Lahiri, S. D., Zhang, G., Dunaway-Mariano, D., and Allen, K. N. (2002) *Biochemistry* **41,** 8351–8359
19. Deshpande, R. A., and Wilson, T. E. (2004) *Biochemistry* **43,** 8579–8589
20. Aravind, L., and Koonin, E. V. (1998) *Trends Biochem. Sci.* **23,** 469–472
21. Omi, R., Goto, M., Nakagawa, N., Miyahara, I., and Hirotsu, K. (2004) *Acta Crystallogr. D. Biol. Crystallogr.* **60,** 574–576
22. Perna, N. T., Plunkett, G. I., Blattner, F. R., Mau, B., and Blattner, F. R. (2001) *Nature* **409,** 529–533
23. Matthews, B. W. (1968) *J. Mol. Biol.* **33,** 491–497
24. Otwinowski, Z., and Minor, W. (1997) *Methods Enzymol.* **276,** 307–326
25. Schneider, T. R., and Sheldrick, G. M. (2002) *Acta Crystallogr. Sect. D. Biol. Crystallogr.* **58,** 1772–1779
26. Sheldrick, G. M. (2002) *Z. Kristallogr.* **217,** 644–650
27. Terwilliger, T. C. (2000) *Acta Crystallogr. Sect. D* **56,** 965–972
28. Perrakis, A., Morris, R., and Lamzin, V. S. (1999) *Nat. Struct. Biol.* **6,** 458–463
29. McRee, D. E. (1999) *J. Struct. Biol.* **125,** 156–165
30. Murshudov, G. N., Vagin, A. A., and Dodson, E. J. (1997) *Acta Crystallogr. Sect. D* **53,** 240–255
31. Laskowski, R. A., MacArthur, M. W., Moss, D. S., and Thornton, J. M. (1993) *J. Appl. Crystallogr.* **26,** 283–291
32. Ames, B. N., Garry, B., and Herzenberg, L. A. (1960) *J. Gen. Microbiol.* **22,** 369–378
33. Van Veldhoven, P. P., and Mannaerts, G. P. (1987) *Anal. Biochem.* **161,** 45–48
34. Selengut, J. D. (2001) *Biochemistry* **40,** 12704–12711
35. Bernstein, N. K., Williams, R. S., Rakovszky, M. L., Cui, D., Green, R., Karimi-Busheri, F., Mani, R. S., Galicia, S., Koch, C. A., Cass, C. E., Durocher, D., Weinfeld, M., and Glover, J. N. (2005) *Mol. Cell* **17,** 657–670
36. Peisach, E., Selengut, J. D., Dunaway-Mariano, D., and Allen, K. N. (2004) *Biochemistry* **43,** 12770–12779
37. Calderone, V., Forleo, C., Benvenuti, M., Cristina, T. M., Maria, R. G., and Mangani, S. (2004) *J. Mol. Biol.* **335,** 761–773
38. Parsons, J. F., Lim, K., Tempczyk, A., Krajewski, W., Eisenstein, E., and Herzberg, O. (2002) *Proteins* **46,** 393–404
39. Lu, Z., Dunaway-Mariano, D., and Allen, K. N. (2005) *Biochemistry* **44,** 8684–8696
40. Yang, W., Lee, J. Y., and Nowotny, M. (2006) *Mol. Cell* **22,** 5–13
41. Peeraer, Y., Rabijns, A., Collet, J. F., Van, S. E., and De, R. C. (2004) *Eur. J. Biochem.* **271,** 3421–3427
42. Wang, W., Cho, H. S., Kim, R., Jancarik, J., Yokota, H., Nguyen, H. H., Grigoriev, I. V., Wemmer, D. E., and Kim, S. H. (2002) *J. Mol. Biol.* **319,** 421–431
43. Shin, D. H., Roberts, A., Jancarik, J., Yokota, H., Kim, R., Wemmer, D. E., and Kim, S. H. (2003) *Protein Sci.* **12,** 1464–1472
44. Sinha, S. C., Chaudhuri, B. N., Burgner, J. W., Yakovleva, G., Davisson, V. J., and Smith, J. L. (2004) *J. Biol. Chem.* **279,** 15491–15498
45. Glynn, S. E., Baker, P. J., Sedelnikova, S. E., Davies, C. L., Eadsforth, T. C., Levy, C. W., Rodgers, H. F., Blackburn, G. M., Hawkes, T. R., Viner, R., and Rice, D. W. (2005) *Structure* **13,** 1809–1817

Structural Snapshots of *Escherichia coli* Histidinol Phosphate Phosphatase along the Reaction Pathway

Erumbi S. Rangarajan, Ariane Proteau, John Wagner, Ming-Ni Hung, Allan Matte and Miroslaw Cygler

J. Biol. Chem. 2006, 281:37930-37941.
doi: 10.1074/jbc.M604916200 originally published online September 11, 2006
